# Magnetic Control of Particle Injection in Plasma Based Accelerators

J. Vieira, S. F. Martins, V. B. Pathak, R. A. Fonseca, W. B. Mori, and L. O. Silva

Phys. Rev. Lett. **106**, 225001 — Published 31 May 2011

DOI: 10.1103/PhysRevLett.106.225001

April 8, 2011

# Magnetic control of particle-injection in plasma based accelerators

J. Vieira[1], S. F. Martins[1], V. B. Pathak[1], R. A. Fonseca[1,2], W.B. Mori[3], and L. O. Silva[1]
[1] *GoLP/Instituto de Plasmas e Fusão Nuclear-Laboratório Associado, Instituto Superior Técnico, 1049-001 Lisboa, Portugal*
[2] *DCTI/ISCTE Lisbon University Institute, 1649-026 Lisbon, Portugal and*
[3] *Department of Physics and Astronomy, UCLA, Los Angeles, California 90095, USA*

The use of an external transverse magnetic field to trigger and to control electron self-injection in laser- and particle-beam driven wakefield accelerators is examined analytically and through full-scale particle-in-cell simulations. A magnetic field can relax the injection threshold and can be used to control main output beam features such as charge, energy, and transverse dynamics in the ion channel associated with the plasma blowout. It is shown that this mechanism could be studied using state-of-the-art magnetic fields in next generation plasma accelerator experiments.

PACS numbers: 41.75.Jv, 52.38.Kd, 52.65Rr, 52.25.Xz

Plasma based acceleration (PBA) has the potential to lead to a future generation of compact particle accelerators. Plasmas sustain electric fields which are more than three orders of magnitude higher than those achieved in any other medium [1]. As standard accelerators reach their technological limits due to the material breakdown thresholds, PBAs promise to push the energy frontier by generating 0.1-1 TeV class electron beams in 1-100 m-scale plasmas [2, 3]. In addition to providing more compact accelerators for high-energy physics, PBA can also provide electron beams for compact radiation sources for medical applications [4], and material science.

Laser wakefield accelerators (LWFAs) deliver 1 GeV class electron bunches with high reproducibility rates [5]. These results were reached in the bubble or blowout regime [6, 7], where the driver pushes plasma electrons radially, leaving an immobile pure ion sphere (bubble) in its path. In this regime, for LWFA, electrons can be self-injected into the wakefield. In contrast, in current plasma wakefield accelerator (PWFA) experiments, self-injection conditions are not easily met as the bubble radius is not as large. Nevertheless, in recent PWFA experiments some electrons had their energy doubled from 42 GeV to 85 GeV in 85 cm [8].

The output controllability is a major challenge for the use of PBA in several applications. To this end, new concepts have emerged such as counter- and cross-propagating laser pulses for LWFA [9], short plasma down-ramps [10], ionization induced trapping [11], and evolving bubbles [12]. With these methods, the charge and energy of self-injected bunches can be adjusted.

In this Letter we propose a novel scheme that uses static transverse magnetic fields to trigger and to control the self-injection in the LWFA or PWFA. The trapping occurs in a local region of the $(\mathbf{p}_\perp, \mathbf{x}_\perp)$ phase-space leading to synchronized betatron oscillations, which could improve the quality of x-ray emission by the magnetically injected electrons [13]. The output energies can also be controlled by adjusting the longitudinal injection position. The scaling law for the magnetic field induced injection is determined with the appropriate Hamiltonian, and illustrated with particle-in-cell (PIC) simulations in OSIRIS [14]. For the next generation PBAs aiming at producing multi-10 GeV electron bunches in controlled injection scenarios [2, 3], our scheme requires external B-fields as low as 5 T.

The use of magnetic fields in PBAs was first explored to reach unlimited particle acceleration in the so-called *surfatron* [15]. The relevance of magnetic fields to PBAs was further examined in [16], while Ref. [17] showed that external longitudinal magnetic fields increase the trapped charge. Our scheme uses an external magnetic field perpendicular to the driver velocity to manipulate self-trapping, generating controlled off-axis injection bursts.

Self-injection can be investigated through the Hamiltonean $H = \sqrt{m_e^2 c^4 + (\mathbf{P} + e\mathbf{A}/c)^2} - e\phi$ for background electrons, where $\mathbf{P} = \mathbf{p} - e\mathbf{A}$ and $\mathbf{p}$ are the canonical and linear momenta, $-e$ the charge of the electron, and $\mathbf{A}$ and $\phi$ the plasma vector and scalar potentials. Unless stated, normalized units are adopted henceforth. Durations are normalized to the inverse of the plasma frequency $\omega_p = \sqrt{4\pi n_0 e^2/m_e}$, lengths to $c/\omega_p$, velocities to $c$, momenta to $m_e c$, and charge to $e$, with $n_0$ the background plasma density, and $m_e$ the electron mass. Vector and scalar potentials are normalized to $e/m_e c^2$ and to $e/m_e c$. The normalized B-field is given by $\omega_c/\omega_p = e|\mathbf{B}|/m_e\omega_p$, and $\omega_c$ is the cyclotron frequency.

In the co-moving frame ($x = x, y = y, \xi = v_\phi t - z, s = z$), the Hamiltonian is $\mathcal{H} = H - v_\phi P_\parallel$, where $v_\phi$ is the plasma wave phase velocity, and $P_\parallel$ is the longitudinal canonical momentum, and it is given by [11, 18]:

$$\frac{\mathrm{d}\mathcal{H}}{\mathrm{d}\xi} = \frac{1}{1 - \frac{v_z}{v_\phi}} \left[ \mathbf{v} \cdot \frac{\partial \mathbf{A}}{\partial s} - \frac{\partial \phi}{\partial s} \right], \qquad (1)$$

where $v_z$ is the electron velocity parallel to the driver velocity. Defining the wake potential as $\psi = \phi - v_\phi A_z$ [18],

and since $v_z = v_\phi$ for trapped electrons, Eq. (1) gives

$$1 + \Delta\psi = \frac{\gamma}{\gamma_\phi^2} - \Delta\mathcal{H}, \tag{2}$$

at the instant of injection, where $\gamma_\phi = (1 - v_\phi^2)^{-1/2}$ is the relativistic factor of the bubble phase velocity, and $\Delta\psi = \psi_f - \psi_i$ ($\Delta\mathcal{H} = \mathcal{H}_f - \mathcal{H}_i$) is the difference between the $\psi$ ($\mathcal{H}$) of the electron at its trapping and initial position. Eq. (2) is consistent with conditions from other electron self-injection mechanisms [11, 12, 18, 20], and is also valid when external fields are present. Considering that $\psi^{\rm ext}$ is related to the external field, and denoting the plasma wave contribution to $\psi$ by $\psi^{\rm pl}$, Eq. (2) becomes:

$$1 + \Delta\psi^{\rm pl} = \frac{\gamma}{\gamma_\phi^2} - \Delta\mathcal{H} - \Delta\psi^{\rm ext}. \tag{3}$$

Eq. (3) shows that self-injection can be relaxed by the presence of external fields. In the absence of external fields ($\Delta\psi^{\rm ext} = 0$) and in the quasi-static approximation [20], such that $\Delta\mathcal{H} = 0$, self-injection occurs when $\Delta\psi^{\rm pl}$ approaches $\Delta\psi^{\rm pl} = -1$ [11, 20, 21]. This condition can be relaxed (i.e. lower $|\Delta\psi|$ can still lead to injection) during the expansion of the wakefield [12] which contributes with finite $\Delta\mathcal{H}$. In the presence of external fields, self-injection may be controlled by acting on $\Delta\mathcal{H}$ and $\Delta\psi^{\rm ext}$. To illustrate the latter mechanism, an external constant magnetic field is considered, and described as $\psi^{\rm ext} = -A_z^{\rm ext} = B_y x$, where $B_y$ is an external B-field pointing in the positive y direction ($B_y > 0$). We also assume that the B-field rises from zero to $B_{y0}$ in a length $L^{\rm ramp}$, is constant for $L^{\rm flat}$, and vanishes in $L^{\rm ramp}$.

We start by investigating trapping in the uniform B-field region when $\gamma_\phi \to \infty$. Eq. (3) then reduces to $1+\Delta\psi^{\rm pl} = -B_{y0}\Delta x$, where $\Delta x = x_f - x_i$ is the difference between the final and initial electron position in the x direction. A conservative threshold B field for injection can be retrieved if we assume that $\Delta\psi = 0$, and that the wake is relatively unperturbed by the B-field as it is the case for $\omega_c/\omega_p \ll 1$. In LWFA matched propagation regimes, the B-injected electrons originate at a distance $x_i \simeq r_b$ from the axis, and they are trapped with $x_f \simeq 0$ [21], thus leading to $\Delta x \simeq -r_b \sin\theta = -2\sqrt{a_0}\sin\theta$, where $r_b = 2\sqrt{a_0}$ is the blowout radius [7], $\theta$ the angle between the plane of the trajectory of the electron with the B-field, and $a_0$ is the normalized laser vector potential. Then, the threshold B-field for injection becomes:

$$B_{y0}^{\rm t} > \frac{\sin\theta}{\sqrt{a_0}}. \tag{4}$$

Eq. (4) illustrates that the external B-field leads to localized off-axis injection in a well defined angular region. We note, however, that since typically $\Delta\psi \lesssim -1$, the assumption $\Delta\psi = 0$ significantly overestimates the required B-field for injection. In fact as we will show in 3D OSIRIS PIC simulations using particle drivers, the threshold B-field for injection is significantly smaller and can be within reach of current technology [19].

The localized injection in the transverse x-y space can also be interpreted in terms of the Larmor rotation of the plasma electrons. Since backward moving electrons in the z-direction rotate anticlockwise for $B_{y0} > 0$, they are bent towards the axis for $x > 0$, entering the accelerating and focusing region of the bubble with larger $p_\parallel$, thus facilitating self-injection. For $x < 0$, electrons move away from the axis, preventing injection. Furthermore, the electrons moving in the plane $x \simeq 0$ are much less disturbed. Hence, the B-field leads to asymmetric trapping which occurs off-axis in a defined angular region.

If $B_y \gg B^{\rm t}$ the plasma wave structure can be significantly modified, which may reduce $|\Delta\psi|$ and $|\Delta x|$, thus suppressing injection. In such cases, however, injection can still occur because the B-field depends on $\xi$. Specifically, as the B-field begins to decrease in the down ramp region then $\psi^{\rm pl}$ returns to its unperturbed state (contribution of the second and third terms on the right-hand-side of Eq. (3)), and $r_b$ gets larger, which effectively lowers $v_\phi$. In the down ramp B-field regions injection also occurs off-axis in a well determined angular region that is identical to that of the self-trapping in uniform B-field regions. It is important to stress that, for the scenarios presented here, the majority of the charge is self-injected in the B-field down ramps. This is the most important mechanism in the present configuration, although for sufficiently large $L^{\rm ramp}$ the mechanisms associated with constant B-fields can also lead to self-injection.

According to Eqs. (2) and (3), higher injection rates occur for higher plasma wave expansion rates, or equivalently for higher B-field down-ramp gradients, i.e. for shorter ramps or higher B's which provide a larger $|\mathbf{v}\cdot\partial\mathbf{A}/\partial s - \partial\phi/\partial s|$ and hence large $|\Delta\mathcal{H}|$. Physically, both tend to lower the phase velocity due to the accordion effect [22]. We note that $L^{\rm ramp}$ can change by modifying the spatial extent of the B-field, and by varying $n_0$.

In order to illustrate this controlled injection mechanism we have performed a set of 3D fully kinetic PIC simulations in OSIRIS [14]. We first consider the LWFA scenario, illustrated in Fig. 1. The simulation box with dimensions of $24 \times 24 \times 12$ $(c/\omega_p)^3$ moves at the speed of light, and is divided into $480 \times 480 \times 1200$ cells with $1 \times 1 \times 2$ electrons per cell in the $(x, y, z)$ directions. The ions form an immobile neutralizing background fluid. A linearly polarized laser pulse with central frequency $\omega_0/\omega_p = 20$ was used, with a peak vector potential of $a_0 = 3$, a duration $\omega_p\tau_{\rm FWHM} = 2\sqrt{a_0}$, and a transverse spot size ($W_0$) matched to the pulse duration such that $W_0 = c\tau_{\rm FWHM}$ [2]. The plasma density is of the form $n = n_0(z)\left(1 + \Delta n r^2\right)$ for $r < \sqrt{10}\ c/\omega_p$ and $n = 0$ for $r > \sqrt{10}c/\omega_p$ with $\Delta n = 4/W_0^4$ being the linear guiding condition, and where $n_0(z)$ is a linear function of $z$ which increases from $n_0 = 0$ to $n_0 = 1$ in 50 $c/\omega_p$ ensuring a

smooth vacuum-plasma transition. The channel guides the front of the laser thereby minimizing the evolution of the bubble. A static external B-field pointing in the positive y-direction was used. At the point where the plasma density reaches its maximum value, the external field rises with $B_y^{\rm ext} = \omega_c/\omega_p = 0.6\sin^2[\pi z/(2L^{\rm ramp})]$, with $L^{\rm ramp} = 10c/\omega_p$, it is constant and equal to $B_{y0}^{\rm ext} = 0.6$ for $L^{\rm flat} = 40\ c/\omega_p$ and drops back to zero with $B_y^{\rm ext} = 0.6\sin^2[\pi z/(2L^{\rm ramp})]$. Considering that the central laser pulse wavelength is 800 nm, this simulation uses a 0.473 J laser pulse, with a spot-size $W_0 = 8.68\ \mu$m, and duration $\tau_{\rm FWHM} = 28.9$ fs. The background plasma density at the bottom of the channel is $n_0 = 4.5\times10^{18}{\rm cm}^{-3}$, and the corresponding B-field is 407 T. While this simulation clearly identified key physical mechanisms associated with the B-field injection using reasonable computational requirements, additional 2D simulations (not shown) revealed that self-injection assisted by magnetic fields can be achieved in the LWFA within state-of-the-art magnetic field generation technology [19]. In Fig. 1a

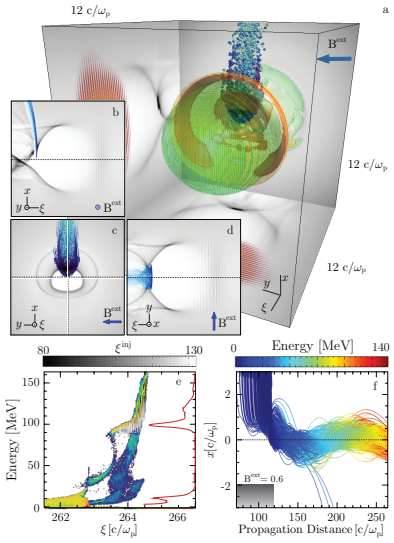


FIG. 1: 3D OSIRIS simulation of a magnetized LWFA. **a**. Electron density iso-surfaces in the uniform B field region. **b-d**. Density profile (gray) associated with the $y = 0$, $\xi = 0$, and $x = 0$ planes of **a** revealing the off-axis injection. Self-injected electrons (darker blue dots) are closer to the bubble axis, while the electrons farther from the bubble axis escape from the trapping region (lighter blue dots). **e**. Phase-space of the plasma electrons (blue-red) and spectrum (red line), showing a quasi-monoenergetic ($\sim 6\%$ FWHM spread) electron bunch. **f**. Trajectories of the self-injected beam particles, with the propagation axis shown by the dashed line. The B-field profile is represented in grayscale.

we plot the electron density, the laser projections (red), and electrons above 10 MeV (blue spheres). Each quantity is plotted when the front of the laser has just left the B-field, at $\omega_p t = 120$, when the laser evolution [23] can be neglected, corresponding to the wake lying entirely within the downramp region. Fig. 1b-d show clearly how the B-field can lead to self-injection. Although the B-field can still decrease $r_b$ in the y-$\xi$, x=0 plane, the wake remains symmetric. This can be seen as follows: when an electron is expelled sideways the B-field provides no extra force. However, as the B-field within the wake bends the trajectory backwards in z, the external B-field (in y) produces a force in the negative x direction. This motion then provides a force in the positive z thereby decreasing $r_b$. On the other hand, the wake is asymmetrically modified in the x-z (y=0) plane. Electrons moving backwards in z feel an downward force from the external B-field. This external force reinforces (reduces) the focusing force for electrons with $x > 0 (x < 0)$. This leads to the sheath structure seen in Fig. 1a. As predicted from Eq. (3), electrons with $\Delta\psi^{ext} < 0$ or equivalently $\Delta x < 0$ are more easily trapped, thus guaranteeing that injection occurs off axis.

The localized trapping provided by the external B-field is also seen in Figs. 1a-c where all electrons above 10 MeV are shown as blue spheres (dots) at $\omega_p t = 120$. The electrons all reside with $x > 0$ and are localized in y as well, i.e., the physics within the x-z plane is dominant. Electrons which eventually reside outsize the wake (large x) are actually defocused by the external B-field. These energetic electrons now move forward in z such that the external B-field leads to a force in the positive x direction. Electrons outside the wake do not feel the focusing force of the wake and therefore are lost.

As the B-field decreases the bubble size increases, effectively decreasing $v_\phi$, leading to an additional and stronger injection. The energy spectrum of the electrons at later propagation distances are shown in Fig. 1e, revealing that a quasi mononergetic beam is formed at $\omega_p t = 270$. The total charge of electrons above 50 MeV is 0.15 nC. In addition, the streaks in Fig. 1e correspond to the trajectories in Energy-$\xi$ phase space, and are plotted for electrons above 50 MeV during the time between 240-270 $\omega_p^{-1}$. The color corresponds to their initial value of $\xi$ ($\xi_{\rm inj}$), then showing that most electrons originate in the downramp region $112 < \xi^{\rm inj} < 122$. Fig. 1f shows that self-injected electrons start with $x > 0$ forming a beam that has a centroid executing betatron oscillations.

In Fig. 2 this scheme is applied to PWFA. The energy of the electron beam is 30 GeV and the density profile is given by $n_b = n_{b0}\exp\left(-\mathbf{x}_\perp^2/(2\sigma_\perp^2)\right)\exp\left(-\xi^2/(2\sigma_z^2)\right)$, where $\sigma_\perp = 0.3\ c/\omega_p$ is the beam transverse spot-size, $\sigma_z = 0.5\ c/\omega_p$ is the beam length, $n_b/n_0 = 8.89$ is the ratio between the beam peak density and background plasma density. For $n_0 = 10^{15}\ {\rm cm}^{-3}$, $\sigma_\perp = 50.4\ \mu$m, $\sigma_z = 84\ \mu$m and to a total number of $3\times10^{10}$ electrons, close to the SLAC electron beam. The simulation box is $12\times12\times16\ (c/\omega_p)^3$, divided into $480\times480\times640$ cells with $2\times2\times1$ particles per cell for the electron beam and background plasma. The B-field profile is similar to the LWFA case with $B_{y0}^{ext} = 0.55\ \omega_c/\omega_p$. For $n_0 =$

$10^{15}$ $cm^{-3}$, this corresponds to $L^{\rm flat} = 6.8$ mm, $L^{\rm ramp} = 1.7$ mm, and $B_{y0}^{\rm ext} = 5.5$ T, within current technological reach [19].

Injection is absent in the unmagnetized PWFA (Fig. 2a-b). In the magnetized case, we observed that self-injection occurs only in the B-field downramp, leading to the generation of a 13 pC electron bunch with 0.1 c/$\omega_p$ = 16.8 $\mu$m long, and 0.2 $c/\omega_p$ = 33.6 $\mu$m wide for $n_0 = 10^{15}$ cm$^{-3}$. As in the LWFA, the deformed structure of the wave only traps plasma electrons located in a narrow angular region (Fig. 2c-d), resulting in synchronized betatron trajectories of the B-injected electrons. We note that the external field also deflects the driver by an angle $\delta \simeq B_y^{\rm ext} L/\gamma_b$, where $L$ is the total B-field length, and $\gamma_b$ is the electron beam relativistic factor. In our scenario, as $\delta \simeq 6 \times 10^{-4}$, the driving beam deflection is negligible, but can still be corrected by placing additional identical external B-fields pointing in the opposite direction. In fact, separating the additional fields by the betatron wavelength can further enhance synchronized injection. To understand the dependence of

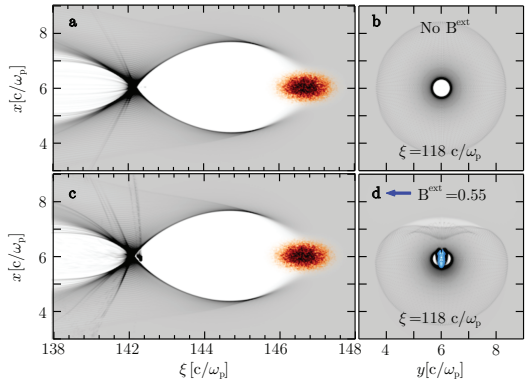


FIG. 2: 3D OSIRIS simulation of B-injection in PWFA (2D slices represented). **a**. Electron density, and **b**. transverse density slice at the back of the bubble in the unmagnetized case. **c**. Electron density after the B-field down-ramp and **d**. Transverse density slice at the back of the bubble, showing trapped particles colored in blue. In **c**. and **d**.

several beam parameters as a function of the B-field down ramp length and amplitude, a 2D parameter scan was performed for the LWFA case (Fig. 3), starting with the parameters associated with Fig. 1, but using $\omega_0/\omega_p = 50$, i.e. more stringent injection conditions. Fig. 3 supports our predictions, showing that the self-injected charge decreases with $L^{\rm ramp}$ (Fig. 3a), and increases with $B_{y0}^{\rm ext}$ (Fig. 3b). The simulations also showed that the self-injected beam radius, energy spread, and beam emittance generally lowers with the applied B-field amplitudes and for shorter ramps. Moreover the beam duration increase for larger B-fields, and for larger field downramps. The injection shutdown occurs for $L^{\rm ramp}$ larger than a few hundred electron skin-depths, corresponding to the cm-mm scale for plasmas with $n_0 = 10^{16} - 10^{17}$ cm$^{-3}$. Finally, these simulations indicate that the threshold B field for injection in the down-ramps is similar to that associated with the uniform B-field region, corresponding to $B_y^{\rm ext} = 1 - 100$ T with $n_0 = 10^{15} - 10^{19}$ cm$^{-3}$. In conclu-

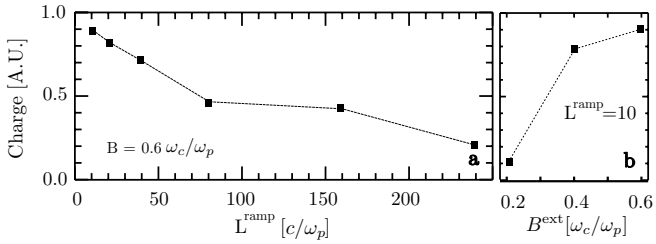


FIG. 3: Parameter scan for the injected charge in the first bucket retrieved from 2D simulations. **a**. Down-ramp length scan, revealing that charge decreases with $L^{\rm ramp}$ **b**. Peak B-field scan, revealing the charge increases with $B_y^{\rm ext}$.

sion, we explored a novel controlled injection mechanism for PBAs, valid for laser- and particle beam drivers. This scheme has the potential to generate high-quality beams in a controlled scenario, since it allows for the tailoring of the injection time period and azimuthal range. It is possible to generate 0.1-1 nC-class electron bunches depending on the plasma and beam density parameters. The plasma, and B-field dependence for the self-injected charge, and self-injection were estimated analytically and are consistent with the results from numerical one-to-one PIC simulations in OSIRIS.

Work partially supported by FCT (Portugal) through grants SFRH/BD/22059/2005, PTDC/FIS/111720/2009, and CERN/FP/116388/2010, EC FP7 through LaserLab-Europe/Laptech; UC Lab Fees Research Award No. 09-LR-05-118764-DOUW, the US DOE under DE-FC02-07ER41500 and DE-FG02-92ER40727, and the NSF under NSF PHY-0904039 and PHY-0936266. Simulations were done on the IST Cluster at IST, on the Jugene supercomputer under a ECFP7 and a DEISA Award, and on Jaguar computer under an INCITE Award.

[1] T. Tajima and J. M. Dawson, Phys. Rev. Lett. **43**, 267 (1979).
[2] W. Lu *et al.*, Phys. Rev. ST Accel. Beams **10**, 061301 (2007).
[3] S.F. Martins *et al.*, Nat. Phys. **6**, pp. 311 - 316(2010).
[4] N. Patel, Nature **449**, 133 (2007).
[5] W. P. Leemans *et al.*, Nat. Phys. **2**, 696 (2006); S. Kneip *et al.*, Phys. Rev. Lett. **103**, 035002 (2009); D. H. Froula *et al.*, Phys. Rev. Lett. **103**, 215006 (2009).
[6] A. Pukhov and J. Meyer ter Vehn, Appl. Phys. B: Lasers Opt. **74**, 355 (2002).
[7] W. Lu *et al.*, Phys. Rev. Lett. **96**, 165002 (2006).

[8] I. Blumenfeld *et al.*, Nature **445**, 741 (2007).
[9] J. Faure *et al.*, Nature **444**, 737 (2006); X. Davoine *et al.*, Phys. Rev. Lett. **102**, 065001 (2009); H. Kotaki *et al.*, Phys. Rev. Lett. **103**, 194803 (2009).
[10] C. G. R. Geddes *et al.*, Phys. Rev. Lett. **100**, 215004 (2008).
[11] A. Pak *et al.*, Phys. Rev. Lett. **104**, 025003 (2010); E. Oz *et al.*, Phys. Rev. Lett. **98**, 084801 (2007).
[12] S. Kalmykov *et al.*, Phys. Rev. Lett. **103**, 135004 (2009).
[13] D. Whittum, A. Sessler, and J. Dawson, Phys. Rev. Lett. **64**, 2511 (1990).
[14] R. A. Fonseca *et al.*, Lect. Notes Comp. Sci. vol. 2331/2002, (Springer Berlin / Heidelberg,(2002).
[15] T. Katsouleas and J. M. Dawson, Phys. Rev. Lett. **51**, 392 (1983).
[16] L. Gorbunov, P. Mora, and T.M. Antonsen Jr., Phys. Rev. Lett. **76**, 2495 (1996); C. Ren and W. B. Mori, Phys. Plasmas **11**, 1978 (2004).
[17] T. Hosokai *et al.*, Phys. Rev. Lett. **97**, 075004 (2006); T. Hosokai *et al.* Appl. Phys. Lett. **96**, 121501 (2010).
[18] W. Lu, PhD Thesis, University of California, Los Angeles (2006).
[19] M. Kumada *et al*, Proceedings of PAC 1993-1995 (2003); B. B. Pollock *et al.*, Rev. Sci. Inst. **77**, 114703 (2006).
[20] E. Esarey and P. Sprangle, IEEE Trans. Plasma Science, **24**, p. 252 (1996) and references therein; P. Sprangle, E. Esarey, and A. Ting, Phys. Rev. Lett. **64**, 2011 (1990); I. Kostyukov *et al.*, Phys. Rev. Lett. **103**, 175003 (2009).
[21] F.S. Tsung *et al.*, Phys. Rev. Lett. **93**, 185002 (2004).
[22] T. Katsouleas, Phys. Rev. A **33**, 2056 (1986).
[23] J. Vieira *et al.*, New J. Phys. **12** 045025 (2010).